Fourth International Symposium on Marine Propulsors
smp'15, Austin, Texas, USA, June 2015

Potential Flow Modelling of Ducted Propellers With a Panel Method

J. Baltazar[1], J.A.C. Falcão de Campos[1], J. Bosschers[2]

[1]Instituto Superior Técnico (IST), Universidade de Lisboa, Portugal
[2]Maritime Research Institute Netherlands (MARIN), Wageningen, the Netherlands

ABSTRACT

The present paper discusses several modelling aspects that are important for the performance predictions of a ducted propeller with a low-order panel method. The aspects discussed are the alignment of the blade wake geometry, the influence of the duct boundary layer on the blade wake pitch, the influence of a transpiration velocity through the gap and the sensitivity to the strength of the shed vorticity from a blunt trailing edge. The analysis is carried out for propeller Ka4-70 operating inside duct 19A. The numerical results are compared with experimental data available from open-water tests. The panel method described in this work gives an acceptable prediction of the open-water characteristics.

Keywords

Ducted Propeller, Panel Method, Kutta Condition, Gap Model, Wake Model.

1 INTRODUCTION

Ducted propellers have been widely used for marine applications. The ability to accurately predict the thrust and torque of a ducted propeller in open-water conditions is very important for a calculation method used in the design stage. Reynolds-averaged Navier-Stokes (RANS) methods are currently being successfully applied for the analysis of the viscous flow around ducted propellers. For example, Abdel-Maksoud and Heinke (2003) and Haimov et al. (2010) have used RANS codes for the performance prediction of a ducted propeller system. Although RANS methods are well-established tools that are able to accurately estimate propeller performance, the computational effort is still reasonably high due to the need of good numerical resolution in small flow regions dominated by strong viscous effects such as in the gap region.

Various numerical methods based on inviscid (potential) flow theory have been proposed for the analysis of ducted propellers. Kerwin et al. (1987) combined a panel method for the duct with a vortex lattice method for the propeller. In this study the influence of the panel arrangement and tip gap was investigated. Later, Hughes (1997) used a panel method for propeller and duct including a gap model for the flow between the blade tip and the duct inner surface. An alternative approach was presented by Gu and Kinnas (2003) using a hybrid method based on a coupling between vortex lattice and finite-volume methods. More recently, Lee and Kinnas (2006) described a panel method for the unsteady flow analysis of a ducted propeller with blade sheet cavitation.

Different numerical studies have been presented comparing the results between panel methods and RANS solvers for ducted propellers (Baltazar et al., 2013; Yu et al., 2013). These studies have shown the limitations in the inviscid flow model when the flow is dominated by the viscous effects, such as the gap flow. From the comparison with the experimental data and RANS calculations, the panel method shows reasonable accuracy in predicting the performance of ducted propellers, when the viscous effects are taken into account in the inviscid model.

This paper focus on the effect of the Kutta condition, gap modelling and wake modelling in the ducted propeller performance predictions with a panel method. The inviscid calculations are made with the IST in-house panel code PROPAN (Baltazar, 2008). The numerical results are compared with open-water data measured at MARIN for the ducted propeller Ka4-70 with $P/D = 1.0$ operating inside duct 19A (Kuiper, 1992). Details of the mathematical formulation of the panel method are given in Section 2. The numerical method is presented in Section 3. The numerical results and the comparison with the experimental data are shown in Section 4. In Section 5 the main conclusions are drawn.

2 MATHEMATICAL FORMULATION

2.1 Potential Flow Problem

Consider a propeller of radius R rotating with constant angular velocity Ω inside a duct and advancing with constant axial speed U along its axis in an incompressible ideal fluid of constant density ρ at rest in a domain extending to infinity in all directions. The propeller is made of K blades symmetrically distributed around an axisymmetric hub. The duct is also considered to be axisymmetric of inner radius at the propeller plane $R_d \geq R$ which defines a gap height $h = R_d - R$. The flow field is steady in a reference frame rotating with the propeller blades around

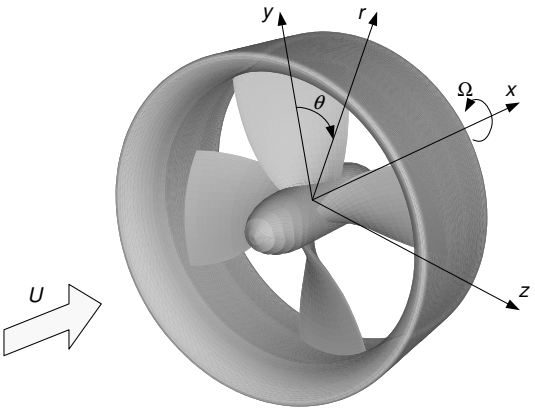

Figure 1: Propeller coordinate system.

its axis. Figure 1 shows the coordinate system used to describe the propeller geometry and the fluid domain around the ducted propeller.

In a Cartesian coordinate system (x, y, z) rotating with the propeller the flow is steady, and under the assumption of irrotational flow the velocity field is described by a perturbation potential ϕ in the form

$$\vec{V} = \vec{U}_\infty + \nabla\phi, \tag{1}$$

where

$$\vec{U}_\infty = U\vec{e}_x + \Omega r\vec{e}_\theta \tag{2}$$

is the undisturbed onset velocity in the rotating frame and $(\vec{e}_x, \vec{e}_r, \vec{e}_\theta)$ are the unit vectors of the cylindrical coordinate system (x, r, θ), with $r = \sqrt{y^2 + z^2}$ and $\theta = \tan^{-1} z/y$. The perturbation potential satisfies the Laplace equation:

$$\nabla^2\phi = 0. \tag{3}$$

The boundary of domain consists of the blade surfaces $\mathcal{S}_\mathcal{B}$, the duct surface $\mathcal{S}_\mathcal{D}$, the hub surface $\mathcal{S}_\mathcal{H}$ and the wake surfaces $\mathcal{S}_\mathcal{W}$ behind the blades and duct. The kinematic boundary condition,

$$\frac{\partial\phi}{\partial n} \equiv \vec{n}\cdot\nabla\phi = -\vec{n}\cdot\vec{U}_\infty \ \text{ on } \ \mathcal{S}_\mathcal{B}\cup\mathcal{S}_\mathcal{D}\cup\mathcal{S}_\mathcal{H}, \tag{4}$$

is satisfied on the blade, duct and hub surfaces, where $\partial/\partial n$ denotes differentiation along the normal and $\vec{n}$ is the unit vector normal to the surface directed outward from the body. At infinity the flow disturbance due to the ducted propeller vanishes $\nabla\phi \to 0$.

The boundary conditions on the wake surfaces $\mathcal{S}_\mathcal{W}$ in steady flow are the tangency of the fluid velocity on each side of the sheet and the continuity of the pressure across the sheet. In order to specify uniquely the circulation around the blades and duct, it is necessary to impose the Kutta condition at the blade trailing edge and at the duct trailing edge. The Kutta condition states that the velocity must remain finite

$$|\nabla\phi| < \infty \tag{5}$$

at a sharp trailing edge. For a round trailing edge this condition is not applicable and an alternative condition must be imposed.

Applying Green's second identity, assuming for the interior region to $\mathcal{S}_\mathcal{B}\cup\mathcal{S}_\mathcal{D}\cup\mathcal{S}_\mathcal{H}$, $\bar{\phi} = 0$, we obtain the integral representation of the perturbation potential at a point p on the body surface,

$$\begin{aligned} 2\pi\phi(p) = &\iint\limits_{\mathcal{S}_\mathcal{B}\cup\mathcal{S}_\mathcal{D}\cup\mathcal{S}_\mathcal{H}} \left[G\frac{\partial\phi}{\partial n_q} - \phi(q)\frac{\partial G}{\partial n_q}\right] dS \\ &- \iint\limits_{\mathcal{S}_\mathcal{W}} \Delta\phi(q)\frac{\partial G}{\partial n_q} dS, \quad p \in \mathcal{S}_\mathcal{B}\cup\mathcal{S}_\mathcal{D}\cup\mathcal{S}_\mathcal{H} \end{aligned} \tag{6}$$

where $G(p,q) = -1/R(p,q)$, $R(p,q)$ is the distance between the field point p and the point q on the boundary $\mathcal{S}_\mathcal{B}\cup\mathcal{S}_\mathcal{D}\cup\mathcal{S}_\mathcal{H}\cup\mathcal{S}_\mathcal{W}$. With the $\partial\phi/\partial n_q$ on the surfaces $\mathcal{S}_\mathcal{B}$, $\mathcal{S}_\mathcal{D}$ and $\mathcal{S}_\mathcal{H}$ known from the Neumann boundary condition on the body surface, Equation (4), the Equation (6) is a Fredholm integral equation of the second kind in the dipole distribution $\mu(q) = -\phi(q)$ on the surfaces $\mathcal{S}_\mathcal{B}$, $\mathcal{S}_\mathcal{D}$ and $\mathcal{S}_\mathcal{H}$. The Kutta condition yields the additional relationship to determine the dipole strength $\Delta\phi(q)$ in the wake surfaces $\mathcal{S}_\mathcal{W}$.

2.2 Velocity, Pressure and Forces

The velocity on the surface is obtained by differentiation of the surface potential distribution. From Bernoulli's equation, the pressure coefficient C_p can be determined from:

$$C_p = \frac{p - p_\infty}{1/2\rho U_\infty^2} = 1 - \left(\frac{|\vec{V}|}{U_\infty}\right)^2, \tag{7}$$

where p is the pressure, p_∞ is the pressure of the undisturbed inflow and $|\vec{V}|$ is the total velocity.

The inviscid thrust and torque on the ducted propeller are obtained by integration of the pressure distribution on the blade and duct surfaces. The propeller operation conditions are defined by a single non-dimensional parameter: the advance coefficient $J = U/(nD)$, where $n = \Omega/2\pi$ is the rate of revolution and $D = 2R$ the propeller diameter. The non-dimensional thrust and torque of the ducted propeller system are given by the propeller thrust coefficient K_{T_P}, the duct thrust coefficient K_{T_D} and the torque coefficient K_Q:

$$K_{T_P} = \frac{T_P}{\rho n^2 D^4}, K_{T_D} = \frac{T_D}{\rho n^2 D^4}, K_Q = \frac{Q}{\rho n^2 D^5}, \tag{8}$$

where T_P is the propeller thrust, T_D the duct thrust and Q the propeller torque. The ducted propeller efficiency is given by $\eta = U(T_P + T_D)/(2\pi nQ)$.

3 NUMERICAL METHOD

3.1 Surface Discretisation

For the numerical solution of the integral equation, Equation (6), we discretise the blade surfaces $\mathcal{S}_\mathcal{B}$, the duct surface $\mathcal{S}_\mathcal{D}$, the hub surface $\mathcal{S}_\mathcal{H}$, and the wake surfaces $\mathcal{S}_\mathcal{W}$ in

bilinear quadrilateral panels. The details of the surface grid generation for the ducted propeller are found in Baltazar (2008).

3.2 Solution of the Integral Equation

The integral equation, Equation (6), is solved by the collocation method with the element centre point as collocation point. We assume a constant strength of the dipole and source distributions on each element. The influence coefficients are determined analytically using the formulations of Morino and Kuo (1974).

3.3 Numerical Kutta Condition

The value of the dipole strength of the wake is determined by the application of a Kutta condition at the blade and duct trailing edges. An iterative pressure Kutta condition imposing equal pressure on both sides of the blade and duct at the trailing edge is considered. This generates a nonlinear system of equations that is solved by the method of Newton and Raphson (Baltazar, 2008). The Morino-Kutta condition is used as a first approximation (Morino and Kuo, 1974).

In the present method, the collocation points of the panels adjacent to the blade trailing edge are used for equality of the pressure on both sides of the propeller blade. From the numerical results for a ducted propeller system using a RANS-based model with the propeller represented by an actuator disk, a pair of counter-rotating vortices at a blunt trailing edge is obtained, following the boundary layer separation on both the outer and inner face of the duct (Hoekstra, 2006). For a blunt round trailing edge it is known that the location of the vortex wake shedding point in the potential flow model strongly influences the circulation around the duct (Baltazar and Falcão de Campos, 2009). This is true both for the Morino and the iterative pressure Kutta condition when applied at the control points adjacent to the vortex wake shedding point. In the present model, the chordwise location for equality of the pressure is not at the vortex wake shedding point but is specified. Its value is interpolated from the computed pressures at the collocation points. The location of the pressure equality points controls the strength of the shed vorticity from duct trailing edge. Due to the possible occurrence of flow separation in the case of a blunt trailing edge, a constant pressure distribution downstream of the Kutta points is assumed in this model. Note that the potential flow solution at the duct trailing edge satisfies the integral equation, Equation (6), but the corresponding pressure distribution is disregarded aft the Kutta points.

3.4 Gap Flow Models

From experimental studies (Oweis et al., 2006) and RANS calculations (Abdel-Maksoud and Heinke, 2003) a complex flow in the gap region of ducted propellers is seen due to the presence and dynamic interactions of the blade wake, tip-leakage vortex, gap flow and duct boundary layer. In the present study, two different models for the potential flow in the gap region are considered: a closed gap with zero gap width and a gap flow model with transpiration velocity. However, these models do not have the ability to represent the details of the flow in the gap region and are used in this work to improve the overall performance predictions of the ducted propeller system.

In the closed gap model, the flow is not allowed to pass between the blade tip and the duct inner surface. In this case, the boundary condition on the gap panels sets the source strength to cancel the normal component of the inflow velocity, Equation (4).

In the gap model with transpiration velocity, a partial flow between the blade tip and the duct inner surface is allowed to pass in the gap region. The procedure proposed by Hughes (1997) is implemented in the current work, where the gap flow is treated as a two-dimensional orifice. In this model, to allow for the existence of a transpiration velocity through the gap, the boundary condition on the gap strip becomes:

$$\frac{\partial \phi}{\partial n} = -\vec{U}_\infty \cdot \vec{n} + |\vec{U}_\infty| C_Q \sqrt{\Delta C_p} \vec{n} \cdot \vec{n}_c, \qquad (9)$$

where $\vec{n}_c$ is the unit normal vector to the mean camber line at the gap strip on the same chordwise position of the panel. The transpiration velocity is prescribed by using a discharge coefficient as originally defined by van Houten (1986). The pressure-difference ΔC_p in the gap panels is obtained by an iterative procedure. Initially, the potential flow problem is solved using the closed gap model. A first approximation of the pressure distribution in the gap strip is obtained. Then, the potential flow problem is solved again using the boundary condition specified by Equation (9). The pressures on the gap strip are then recomputed and its value updated in the boundary condition, Equation (9). The solution process is repeated until a specified convergence criterion is met.

3.5 Wake Models

The importance of the blade wake geometry on the performance prediction with a panel method for both open and ducted propellers has been widely emphasised and there is already considerable literature on this subject (Lee and Kinnas, 2005; Baltazar et al., 2012). In the present work, two wake models are considered: a rigid wake model and a wake alignment model for the blade wake where the pitch of the vortex lines is aligned with the local fluid velocity.

In the rigid wake model, the geometry of the wake surfaces is specified empirically. For the blade wake, the pitch of the vortex lines is assumed constant along the axial direction and equal to the blade pitch. For the duct, the wake leaves the trailing edge at the bisector.

In the wake alignment model, the corner points of the blade wake panels are displaced with the mean fluid velocity. In

this model, the radial coordinates of the blade wake panels are kept constant and only the pitch of the vortex lines is aligned with the mean fluid velocity. Then, the new axial and circumferential coordinates $x_{i+1}^{(n+1)}$ and $\theta_{i+1}^{(n+1)}$ of the wake strip $i+1$ at the $(n+1)$th iteration are determined by using an Euler scheme:

$$\begin{cases} x_{i+1}^{(n+1)} = x_i^{(n)} + V_x\left(x_i^{(n)}, r_i^{(n)}, \theta_i^{(n)}\right)\Delta t \\ \theta_{i+1}^{(n+1)} = \theta_i^{(n)} + V_\theta\left(x_i^{(n)}, r_i^{(n)}, \theta_i^{(n)}\right)\Big/ r_i^{(n)}\Delta t \end{cases}, \tag{10}$$

where V_x and V_θ are the components of the mean vortex sheet velocity along the axial and circumferential directions, respectively, and Δt is the time step for the Euler vortex convection scheme. The velocity components are calculated from the integral equation of the velocity, obtained by taking the gradient of Equation (6). The non-dimensional time step $\Delta\theta = \Omega\Delta t$ is introduced, which can also be expressed in terms of the number of time steps per propeller revolution $N_\theta = 2\pi/\Delta\theta$.

3.6 Model for the Interaction of the Blade Wake With the Duct Boundary Layer

In combination with the wake alignment model, a simple model for the interaction between the blade wake and the boundary layer on the duct inner side is implemented as well. Due to the duct boundary layer, a reduction in the axial velocity may be taken into account in the convection of the blade vorticity in the wake alignment model. Considering δ as the duct boundary layer thickness and assuming a power law distribution for the velocity profile, we have

$$\frac{V_x\left(R_d - r\right)}{V_x\left(\delta\right)} = \left(\frac{R_d - r}{\delta}\right)^{\frac{1}{n}}. \tag{11}$$

To avoid zero axial velocity at the duct inner surface, its value is obtained by extrapolation from the axial velocity at the gap $V_x(h)$, and at the edge of the duct boundary layer $V_x(\delta)$. The reduction in the blade wake pitch near the tip due to the interaction between the duct boundary layer and the propeller blades changes the incidence angle to the blade sections and influences the propeller performance predictions (Baltazar et al., 2012). This effect has been the subject of investigation on the operating characteristics of different types of turbo-machines. One of the first studies was carried out by Boxer (1951) for an axial-flow fan rotor, where a similar effect was found due to the wall boundary layer.

4 RESULTS

4.1 General

Results are presented for the propeller Ka4-70 inside the duct 19A. The propeller Ka4-70 is a four-bladed propeller of the Kaplan type. A pitch-diameter ratio of $P/D = 1.0$ is considered. The duct 19A has an axial cylindrical part in the inner side of the duct at the propeller location. The outer side of the duct is straight and the trailing edge of the duct is round. This duct has a length-diameter ratio of 0.5. The gap between the duct inner side and the blade tip is uniform and equal to 0.8% of the propeller radius. The particulars of the Ka-series and the duct section geometry can be found in Kuiper (1992). Figure 2 shows a typical panel arrangement of propeller Ka-470 inside the duct 19A with an open-water hub.

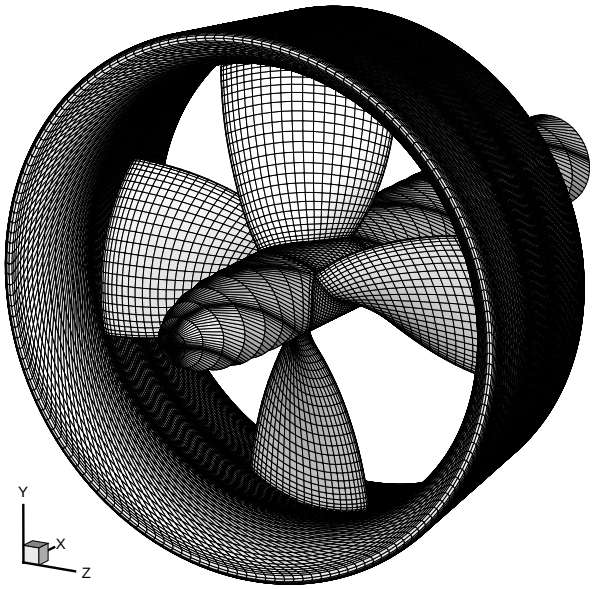

Figure 2: Panel arrangement for propeller Ka4-70 inside duct 19A. 50×25 panels on each blade; 190×160 panels on the duct; 55×80 panels on the hub.

4.2 Influence of the Kutta Condition

The influence of the pressure equality points at the duct trailing edge is investigated. A specified tolerance of $|\Delta C_p|_{TE} \leq 10^{-3}$ for the pressure-jump at the control points is applied. In this case, the closed gap is used to model the gap flow and the rigid wake model for the blade wake. Eight different locations are considered, varying from 96.5% to 100% of the duct length. The location of the pressure equality points at 99.9% of the duct length corresponds to the collocation points of the panels adjacent to the duct trailing edge. Figure 3 shows the trailing edge of the duct 19A with the location of the pressure equality points.

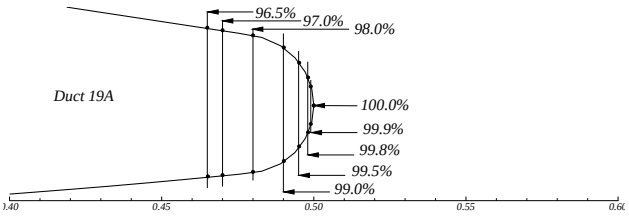

Figure 3: Location of the pressure equality points as percentage of the duct length.

The influence on the inviscid thrust and torque for $J = 0.2$ and $J = 0.5$ is given in Table 1. A strong influence on

Table 1: Inviscid thrust and torque coefficients for $J = 0.2$ and $J = 0.5$. Influence of the pressure equality location at the duct trailing edge.

J	0.2			0.5		
Location	K_{T_P}	K_{T_D}	$10K_Q$	K_{T_P}	K_{T_D}	$10K_Q$
100.0%	0.221	0.142	0.341	0.157	0.060	0.250
99.9%	0.287	0.163	0.432	0.199	0.067	0.311
99.8%	0.315	0.165	0.468	0.215	0.066	0.335
99.5%	0.357	0.165	0.521	0.241	0.062	0.370
99.0%	0.387	0.159	0.559	0.262	0.053	0.399
98.0%	0.388	0.159	0.560	0.268	0.053	0.407
97.0%	0.359	0.167	0.524	0.255	0.061	0.390
96.5%	0.351	0.168	0.515	0.252	0.062	0.386

the propeller forces due to the chordwise position that imposes equal pressure on both sides is seen. A maximum for the propeller thrust and torque is found at 98% of the duct length. An opposite effect is obtained for the duct thrust. We note that the transition from the straight parts of the duct inner and outer surfaces to the round geometry of the trailing edge occurs approximately at 98% of the duct length. The assumption for the points at the upper and lower sides of the duct at this location as flow separation points seems a reasonable approximation in the proposed model. In the present work, special attention is given to the 98% duct length location.

4.3 Influence of the Gap Model

In this section the influence of the gap model on the potential flow solution is studied. The gap model is implemented by setting different values for the discharge coefficient C_Q. The closed gap model is simulated by setting $C_Q = 0.0$, which imposes the zero normal boundary condition in the gap strips. Values of the discharge coefficient equal to 0.5, 0.84, 1.0, 2.0 and 5.0 are also considered. The discharge coefficient equal to 0.84 represents the mean of the values compiled by van Houten (1986). The assumption of $C_Q = 1.0$ represents the case where there is no loss of energy as the fluid passes through the gap. By increasing the discharge coefficient to values larger than 1.0, the flow tends to the inviscid solution without gap. In this study, this case is modelled by setting $C_Q = 5.0$. A tolerance of 10^{-2} for the variation of the pressure-difference on the gap strip control points is applied as convergence criterion of the gap model. Calculations are carried out using the rigid wake model and assuming for the duct Kutta condition the location at 98.0% of the duct chord.

The influence of the discharge coefficient on the inviscid thrust and torque for $J = 0.2$ and $J = 0.5$ is given in Table 2. The results show a small effect on the propeller and duct forces for values of the discharge coefficient between 0.0 and 1.0. A larger variation is obtained when increasing the discharge coefficient to values higher than 1.0. Figure 4 presents the circulation distribution on the propeller blade,

Table 2: Inviscid thrust and torque coefficients for $J = 0.2$ and $J = 0.5$. Influence of the discharge coefficient.

J	0.2			0.5		
C_Q	K_{T_P}	K_{T_D}	$10K_Q$	K_{T_P}	K_{T_D}	$10K_Q$
5.00	0.370	0.115	0.529	0.251	0.027	0.380
2.00	0.373	0.144	0.539	0.254	0.045	0.387
1.00	0.379	0.152	0.548	0.261	0.050	0.397
0.84	0.380	0.154	0.550	0.262	0.051	0.399
0.50	0.383	0.156	0.554	0.264	0.052	0.402
0.00	0.388	0.159	0.560	0.268	0.053	0.407

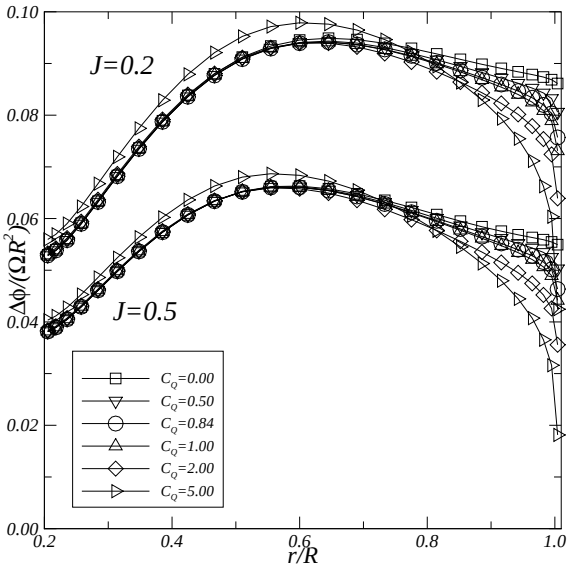

Figure 4: Influence of the discharge coefficient on the blade circulation distribution for $J = 0.2$ and $J = 0.5$.

where a small influence of the gap model is seen near the blade tip for discharge coefficients between 0.0 and 1.0. In the closed gap model ($C_Q = 0.0$), a finite circulation at the blade tip is obtained. By increasing the discharge coefficient, a reduction in the tip circulation is seen. This study suggests that no significant improvement on the ducted propeller performance predictions is obtained by imposing a transpiration velocity in the gap region, since similar results are achieved with the closed gap model. For discharge coefficients higher than 1.0 the blade tip circulation tends to zero.

4.4 Influence of the Wake Model

In this section the influence of the wake model is studied. Results are presented using three wake models: rigid wake model, wake alignment model (WAM) for the blade wake and wake alignment model for the blade wake using the duct boundary layer correction. The wake geometries are obtained after 5 iterations of the wake alignment model using $N_\theta = 90$ time steps per revolution, giving an angular step of 4 degrees. For the duct boundary layer correction model a thickness equal to $\delta/R = 4\%$ is assumed, corre-

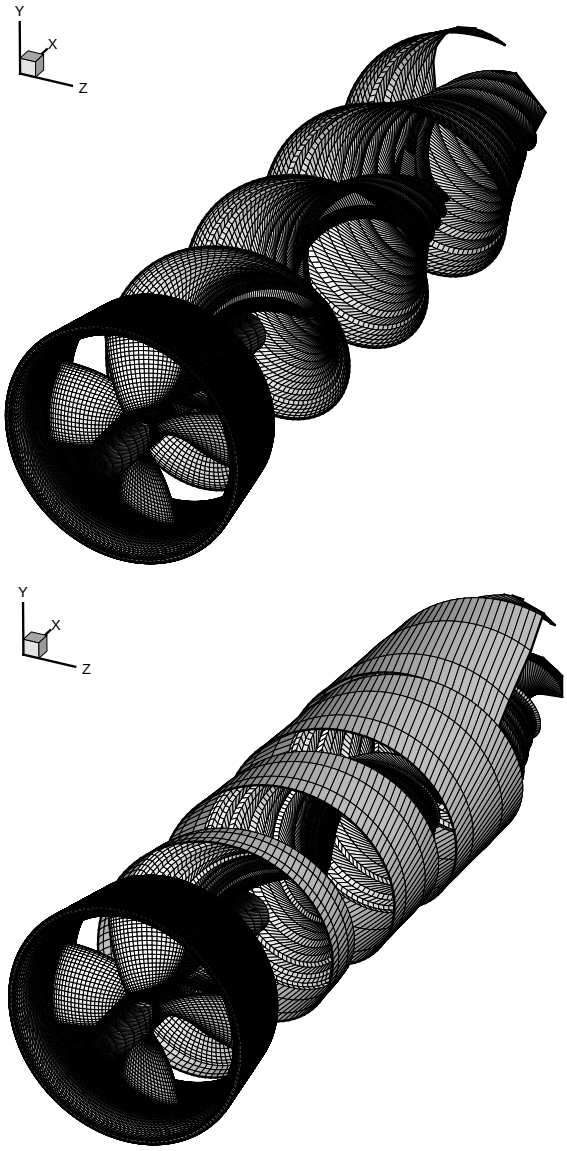

Figure 5: Panel arrangement for propeller blades, duct and blade wake at $J = 0.2$. Wake alignment model (top). Wake alignment model with duct boundary layer correction (bottom). Only one wake surface shown.

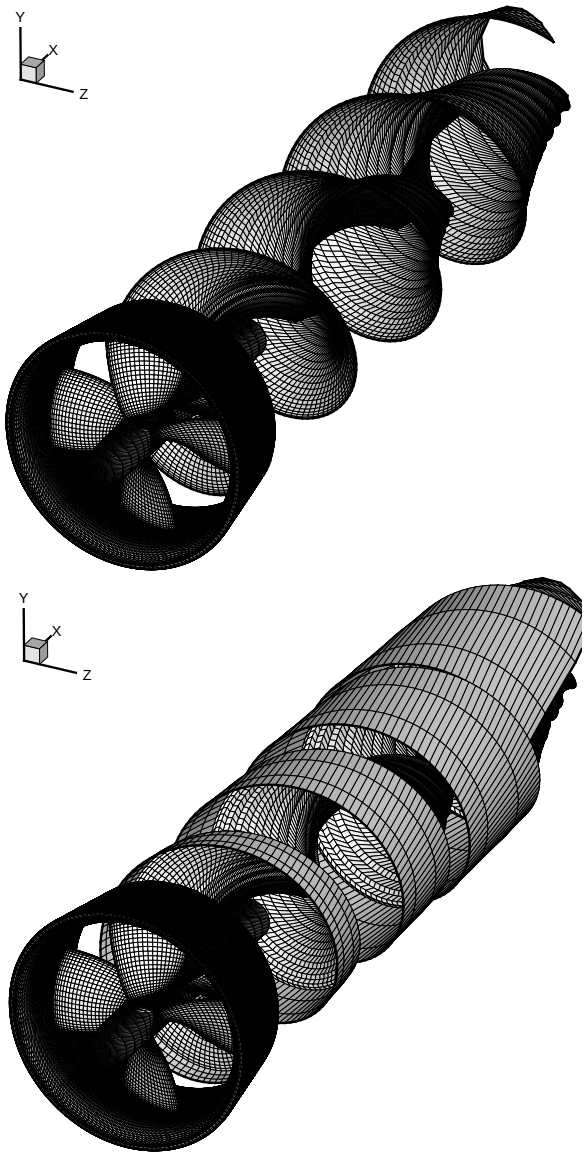

Figure 6: Panel arrangement for propeller blades, duct and blade wake at $J = 0.5$. Wake alignment model (top). Wake alignment model with duct boundary layer correction (bottom). Only one wake surface shown.

sponding to $h/\delta = 0.21$. A power law velocity profile with $n = 7$ is also assumed. For the duct Kutta condition, the location at 98.0% of the duct length is used for pressure equality. The closed gap model is used to model the gap flow.

Figures 5 and 6 presents the panel arrangements obtained with the wake alignment model without and with duct boundary layer thickness for $J = 0.2$ and $J = 0.5$, respectively. Smooth blade wake geometries are obtained with the wake alignment model. As it may be clearly seen in the figures, the correction in the axial velocity due to the duct boundary layer introduces a significant reduction in the vortex pitch at the blade wake tip.

Figures 7 and 8 present the pressure distributions on the propeller blade and duct for $J = 0.2$ and $J = 0.5$, respectively. The pressure distributions are shown as function of the chordwise position s/c, where s is defined along the cylindrical section chord for the propeller blade and as the axial distance along the meridional duct section from leading edge to trailing edge. For the blade pressure distribution, a smaller suction peak is obtained with the wake alignment model with the duct boundary layer, indicating a lower incidence angle to the blade section near the tip. For the duct pressure, a uniform distribution is seen near the trailing edge. This result is due to the Kutta condition model, which assumes a constant pressure distribution from the pressure equality points to the duct trailing edge.

The influence of the wake model on the inviscid thrust and torque for $J = 0.2$ and $J = 0.5$ is given in Table 3. Results are presented for the rigid wake model (RW), wake alignment model, corresponding to $\delta/R = 0$, and the wake alignment model with duct boundary layer cor-

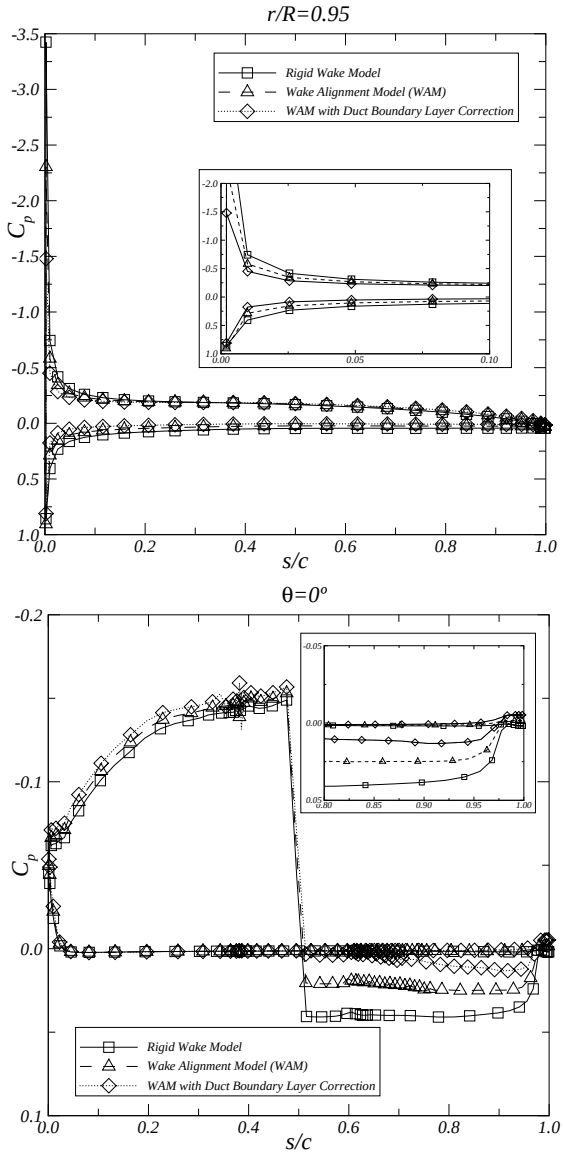

Figure 7: Blade chordwise pressure distribution at $r/R = 0.95$ (top). Duct chordwise pressure distribution at $\theta = 0$ degrees (bottom). Influence of the wake model at $J = 0.2$.

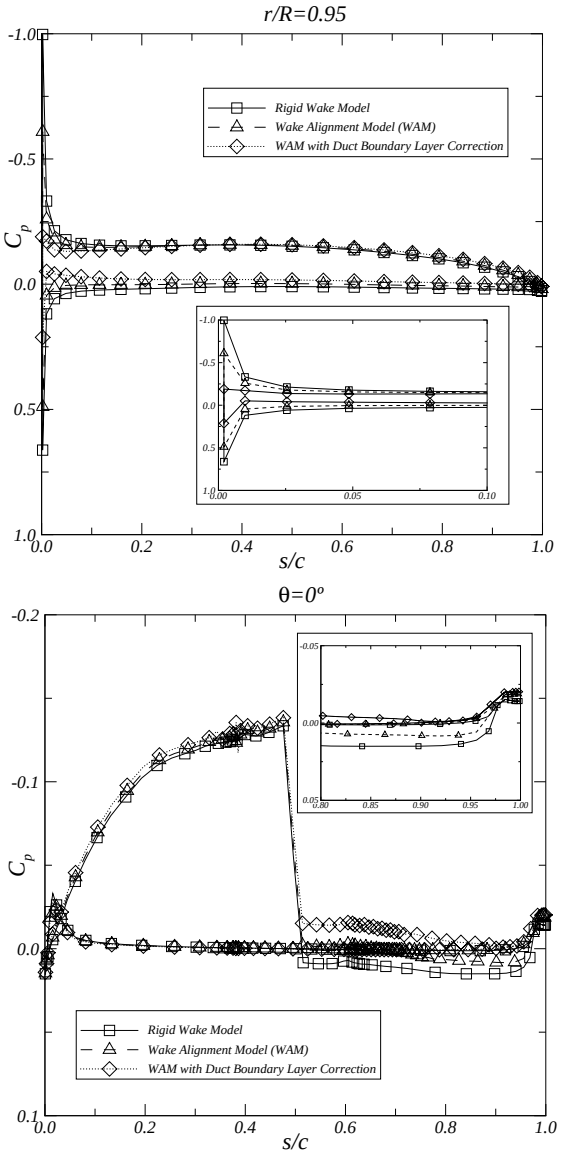

Figure 8: Blade chordwise pressure distribution at $r/R = 0.95$ (top). Duct chordwise pressure distribution at $\theta = 0$ degrees (bottom). Influence of the wake model at $J = 0.5$.

rection, where the duct boundary layer thickness ranges from 1% to 5%. Although the correction due to the duct boundary layer affects only the blade wake geometry near the tip, a strong influence on the ducted propeller forces is obtained. It is seen that an increase in the boundary layer thickness leads to a reduction of the propeller thrust and torque.

4.5 Comparison With Experimental Data

In this section, the predicted thrust and torque coefficients are compared with experimental data from open-water tests (Kuiper, 1992). Calculations are presented for the wake alignment model with a constant duct boundary layer of $\delta/R = 4\%$. For the duct Kutta condition three different positions for pressure equality are considered: 97%, 98% and 99% of the duct length. Figure 9 illustrates the comparison of the thrust and torque coefficients with the experiments. A section viscous drag coefficient of 0.007 and suppression of the chordwise component of the blade section are used for all computations. This suppression models the effect of flow separation which eliminates the unphysical suction peaks at the leading edge in the potential flow theory. No viscous drag correction to the duct thrust has been applied. We note that the wake alignment model converged for all advance ratios of the open-water diagram.

Similar results are obtained with the three pressure equality positions assumed for the duct trailing edge. This results show a small influence on the duct loading for the range between 97% and 99% of the duct length. From RANS computations (Hoekstra, 2006; Yu et al., 2013), the assumption of a constant pressure equality position along the circum-

Table 3: Inviscid thrust and torque coefficients for $J = 0.2$ and $J = 0.5$. Influence of the wake model.

J	0.2			0.5		
Wake	K_{T_P}	K_{T_D}	$10K_Q$	K_{T_P}	K_{T_D}	$10K_Q$
RW	0.388	0.159	0.560	0.268	0.053	0.407
δ/R=0%	0.341	0.167	0.503	0.242	0.054	0.372
δ/R=1%	0.322	0.172	0.478	0.231	0.055	0.357
δ/R=2%	0.310	0.173	0.462	0.212	0.058	0.331
δ/R=3%	0.305	0.174	0.456	0.211	0.058	0.328
δ/R=4%	0.301	0.175	0.452	0.211	0.056	0.329
δ/R=5%	0.295	0.177	0.443	0.205	0.058	0.321

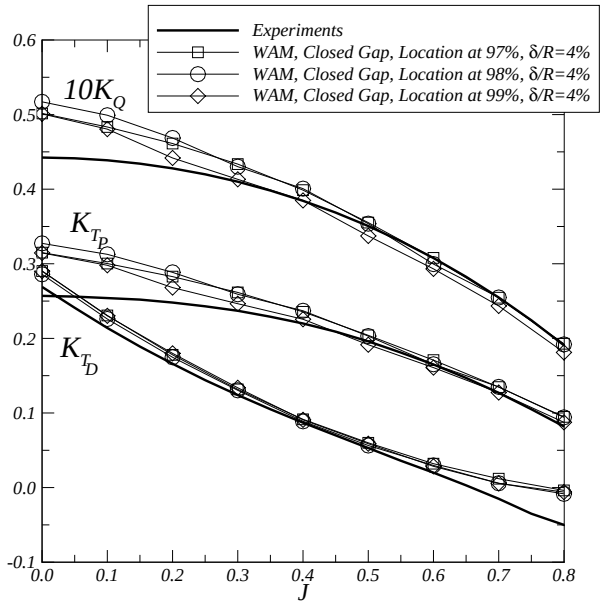

Figure 9: Open-water diagram. Comparison between numerical and experimental results.

ferential direction and the independence from the inflow conditions is questionable. Still, the propeller thrust and torque are well predicted for the advance ratios higher than 0.3. The duct thrust coefficient agrees well with the measurements for low advance coefficients. For high advance coefficients, an over-prediction of the duct thrust is seen, which is probably due to the occurrence of flow separation on the outer side of the duct and it is not modelled in the present method. The differences between the measured and the predicted ducted propeller efficiencies are around 5% for the advance ratios lower than 0.6.

5 CONCLUSIONS

A low-order panel method has been used to predict the thrust and torque of propeller Ka-470 inside duct 19A in open-water conditions. The influence of the Kutta condition for a blunt trailing edge, the modelling of the gap flow between the propeller blade tip and the duct inner side, and the alignment of the blade wake sheet are analysed in this paper. The numerical results are compared with experimental data from open-water tests. Based on the numerical results obtained for the ducted propeller system, the following conclusions are drawn:

- For a blunt trailing edge, flow separation is expected to occur due to a rapid variation of geometry. For the duct 19A, the geometry changes from a straight shape to a round shape near 98% of its length. In this study an alternative duct Kutta condition model is proposed, where the chordwise location of pressure equality on both sides is specified. This location is found to have a strong influence on the propeller forces.

- The model of the gap flow between the tip of the propeller and the duct inner side is necessary for an accurate prediction of the propeller forces using a panel method, since large differences in the forces predictions are obtained from the comparison between a closed gap model and a open gap. Results are compared with a gap flow model using a transpiration velocity for the gap region, where a small influence on the propeller and duct forces is found. Accordingly, the use of a closed gap model appears sufficient for an accurate prediction of the ducted propeller forces.

- A strong influence of the blade wake pitch, especially near the blade tip, on the ducted propeller force predictions is seen. A simple model to account for the influence of the duct boundary layer on the pitch of the tip vorticity is implemented. However, a large variation on the force predictions due to the duct boundary layer thickness is found and a careful tuning is therefore needed to correctly predict the open-water characteristics.

- In this case, the use of a low-order panel method, in combination with an alternative Kutta condition for the duct trailing edge, with a closed gap model and with a wake alignment model for the blade wake sheet gives an acceptable prediction of the open-water characteristics.

REFERENCES

Abdel-Maksoud, M. and Heinke, H.-J. (2003). 'Scale effects on ducted propellers'. In Proceedings of the Twenty-Fourth Symposium on Naval Hydrodynamics, Fukuoka, Japan.

Baltazar, J. (2008). On the Modelling of the Potential Flow About Wings and Marine Propellers Using a Boundary Element Method. PhD thesis, Instituto Superior Técnico.

Baltazar, J. and Falcão de Campos, J. A. C. (2009). 'On the modelling of the flow in ducted proopellers with a panel method'. In Proceedings of the 1st International Symposium on Marine Propulsors, Trondheim, Norway.

Baltazar, J., Falcão de Campos, J. A. C., and Bosschers, J. (2012). 'Open-water thrust and torque predictions of a ducted propeller system with a panel method'. International Journal of Rotating Machinery, Article ID 474785.

Baltazar, J., Rijpkema, D., Falcão de Campos, J. A. C., and Bosschers, J. (2013). 'A comparison of panel method and RANS calculations for a ducted propeller system in open-water'. In Proceedings of the 3rd International Symposium on Marine Propulsors, Launceston, Tasmania, Australia.

Boxer, E. (1951). 'Influence of wall boundary layer upon the performance of an axial-flow fan rotor'. Technical Note 2291, National Advisory Committee for Aeronautics.

Gu, H. and Kinnas, S. A. (2003). 'Modeling of contra-rotating and ducted propellers via coupling of a vortex-lattice with a finite volume method'. In Proceedings of the Propellers/Shafting 2003 Symposium, Virginia Beach, Va, USA.

Haimov, H., Bobo, M. J., Vicario, J., and del Corral, J. (2010). 'Ducted propellers. A solution for better propulsion of ships. Calculations and practice'. In Proceedings of the 1st International Symposium on Fishing Vessel Energy Efficiency E-Fishing, Vigo, Spain.

Hoekstra, M. (2006). 'A RANS-based analysis tool for ducted propeller systems in open water condition'. International Shipbuilding Progress, 53:205 – 227.

Hughes, M. J. (1997). 'Implementation of a special procedure for modeling the tip clearance flow in a panel method for ducted propelelrs'. In Proceedings of the Propellers/Shafting '97 Symposium, Virginia Beach, Va, USA.

Kerwin, J. E., Kinnas, S. A., Lee, J.-T., and Shih, W.-Z. (1987). 'A surface panel method for the hydrodynamic analysis of ducted propellers'. Transactions of Society of Naval Architects and Marine Engineers, 95.

Kuiper, G. (1992). The Wageningen Propeller Series. MARIN Publication 92-001.

Lee, H. and Kinnas, S. A. (2005). 'Unsteady wake alignment for propellers in nonaxisymmetric flows'. Journal of Ship Research, 49(3):176 – 190.

Lee, H. and Kinnas, S. A. (2006). 'Prediction of cavitating performance of ducted propellers'. Proceedings of the Sixth International Symposium on Cavitation.

Morino, L. and Kuo, C.-C. (1974). 'Subsonic potential aerodynamics for complex configurations: a general theory'. AIAA Journal, 12(2):191 – 197.

Oweis, G. F., Fry, D., Chesnakas, C. J., Jessup, S. D., and Ceccio, S. L. (2006). 'Development of a tip-leakage flow–Part 1: the flow over a range of Reynolds numbers'. Journal of Fluids Engineering, 128(4):751 – 764.

van Houten, R. (1986). 'Analysis of ducted propellers in steady flow'. Technical Report 4.76-1, Airflow Research and Manufacturing Corp.

Yu, L., Martin, G., Druckenbrod, M., and Abdel-Maksoud, M. (2013). 'Numerical analysis of ducted propeller performance under open water test condition'. Journal Marine Science Technology, 18(3):381 – 394.

DISCUSSION

Questions from Ye Tian

The duct boundary layer thickness δ showed strong effect on the solution. How can this δ be determined without trial-and-error, matching K_T/K_Q with experimental data? Is there any correlation between the best fitted δ in the BEM and that observed from RANS simulation? For the wake alignment model, the paper says that "the corner points of the blade wake panels are displaced with the mean fluid velocity". Please clarify what is the "mean fluid velocity". For the wake alignment model, how many iterations are usually needed?

Authors' Closure

Thank you for your questions. For the specification of the duct boundary layer thickness δ, an empirical correlation may be developed from the experimental results of the Ka series. In the present work, the order of magnitude of the duct boundary layer thickness at the propeller plane was first estimated from the equation for a turbulent boundary layer over a flat plate. Then the assumption of $\delta/R = 4\%$ was obtained after a sensitivity study on the influence of the duct boundary layer thickness on the predicted thrust and torque coefficients. The boundary layer characteristics have not yet been analysed from RANS simulations for the Ka series. For the wake alignment model, the "mean fluid velocity" denotes the average velocity across the wake vortex sheet. For the iterative alignment of the wake, between 3 to 5 iterations are needed for convergence of the blade wake geometry. In the present work, all blade wakes are obtained after 5 iterations of the wake alignment model.